Relay-Aided Wireless Sensor Network Discovery Algorithm for Dense Industrial IoT Utilizing ESPAR Antennas

Fjolla Ademaj, *Member, IEEE*, Mateusz Rzymowski, *Member, IEEE*, Hans-Peter Bernhard, *Senior Member, IEEE*, Krzysztof Nyka, *Senior Member, IEEE*, and Lukasz Kulas, *Senior Member, IEEE*

***Abstract*—Industrial Internet-of-Things (IIoT) applications require reliable and efficient wireless communication. Assuming dense wireless sensor networks (WSNs) operating in a harsh environment, a concept of a time-division multiple access (TDMA)-based WSN enriched with electronically steerable parasitic array radiator (ESPAR) antennas is proposed and examined in this work. The utilized antenna provides one omnidirectional and 12 directional radiation patterns that can be electronically switched by the sensor node. We introduce a relay discovery algorithm, which selects those sensor nodes with an ESPAR antenna capable to act as relay. The selection of the relay nodes is based on a certain link quality threshold that algorithm uses as input. The outcome is a reduction in the number of layers or hops with a guaranteed Quality of Service (QoS). To emphasize the physical aspect of the wireless propagation, we introduce the measured antenna radiation patterns and consider two different path-loss propagation models representing blockage-free and blockage-prone industrial environments. A number of network simulations were performed and signal-to-noise ratio (SNR) as a link quality measure was examined with respect to the network density and different measured radiation pattern settings. The main outcomes show a tradeoff between SNR per link and the percentage of nodes that can serve as relays. As a result, we propose network design guidelines that take under consideration the QoS range with respect to SNR together with an optimal number of antenna radiation patterns that should be selected as a tradeoff between latency, energy consumption, and reliability in a network.**

***Index Terms*—Electronically steerable parasitic array radiator (ESPAR), Industrial Internet of Things (IIoT), multihop communication, Quality of Service (QoS), relay, routing, switched-beam antenna, wireless sensor networks (WSNs).**

I. Introduction

THE INDUSTRY 4.0 paradigm relies on ubiquitous connectivity between devices to maximize the information about automation processes in order to optimize them [1], [2] . One of the key concepts developed nowadays to enable this is the Industrial Internet of Things (IIoT), where machinery equipped with a number of interconnected sensors and actuators control their efficient operation or in some cases can even support safety-critical systems [3]–[5]. For this reason, reliable, secure, and dependable wireless communication has to be provided [6]–[8]. The network structure in Industrial Internet of Things (IIoT) is centralized, where sensor nodes have fixed locations and are centrally managed by a controlling unit. Nevertheless, the industrial sites are usually very demanding with respect to wireless communication due to the multipath propagation and reflections caused by the presence of metal objects or other obstacles and dynamically changing environmental conditions caused by moving objects. Dense wireless networks operating in such spaces can also result in co-existence problems, where different nodes can interfere with each other. For this reason, providing stable and reliable communication parameters in such an environment is very challenging and has already been broadly addressed in the literature by proposing nonstandard systems with dedicated protocols and using various routing algorithms [9]–[13]. Nobre *et al.* [14] provided a detailed survey on routing algorithms for IIoT, emphasizing graph routing approaches that address network lifetime, latency, and energy consumption. Other research have proven that there are some limitations that cannot be mitigated only with the changes on higher protocol layers and need considering improvements on the physical layer as well [15]–[17]. This is usually achieved by adjusting the properties of physical radio-frequency (RF) signals to the propagation environments and distribution of wireless sensors. The simplest yet effective approach is to equip IIoT nodes with additional spatial diversity capabilities

Manuscript received December 24, 2020; revised February 25, 2021 and March 29, 2021; accepted April 17, 2021. Date of publication April 23, 2021; date of current version November 5, 2021. This work was supported in part by the InSecTT Project (https://www.insectt.eu/) through the ECSEL Joint Undertaking (JU) under Grant 876038. The JU receives support from the European Union's Horizon 2020 research and innovation programme and Austria, Sweden, Spain, Italy, France, Portugal, Ireland, Finland, Slovenia, Poland, Netherlands, Turkey. *(Corresponding author: Fjolla Ademaj.)*

Fjolla Ademaj is with the Research Unit Wireless Communications, Silicon Austria Labs GmbH, 8010 Graz, Austria (e-mail: fjolla.ademaj@silicon-austria.com).

Mateusz Rzymowski, Krzysztof Nyka, and Lukasz Kulas are with the Department of Microwave and Antenna Engineering, Gdansk University of Technology, 80-233 Gdansk, Poland (e-mail: mateusz.rzymowski@pg.edu.pl; krznyka@pg.edu.pl; lukasz.kulas@eti.pg.gda.pl).

Hans-Peter Bernhard is with Silicon Austria Labs GmbH, 4040 Linz, Austria, and also with the Institute for Communications Engineering and RF-Systems, Johannes Kepler University Linz, 4040 Linz, Austria (e-mail: h.p.bernhard@ieee.org).

Digital Object Identifier 10.1109/JIOT.2021.3075346

usually realized by dedicated antennas that can change their parameters to better fit into a given environment or network operation scenario. The directional antennas having controllable radiation patterns and gain values can improve the link quality [18]–[20]. Different approaches that use directional antennas to improve the network parameters has been proposed in the literature [21]–[25]. The narrow directional beam and high gain of the antenna allow increasing the communication range and limiting the signal coverage area, which can reduce the risk of potential interference. However, the proposed protocols that are based on the directional antennas report a number of negative aspects that have to be considered, such as the hidden terminal problem, deafness, neighbor discovery, etc., and potential ways to mitigate them by proper mechanisms on the medium access control (MAC) layer [26]. It has to be noted, however, that solutions proposed so far were mostly evaluated with network simulators that do not take into account physical phenomena related to propagation. Although the presented results give an outstanding view of the whole network operation, a simplified physical-layer emulation used therein may be insufficient with respect to the real network behavior in harsh and dynamically changing propagation environments. This arises the need for a deeper examination of the network operation with respect to the propagation phenomena within indoor spaces, especially those of industrial sites. The directional antennas that provide one fixed radiation pattern may not allow for an optimal operation in the case of dynamically changing environment conditions and nonstatic network topology. For this reason, different concepts of reconfigurable antennas have been proposed [27], [28]. Such antennas give ability to electrically control their radiation pattern using different approaches from simple switching to advanced beamforming techniques. In the case of dense wireless sensor networks (WSNs), the cost and energy efficiency are the key parameters, so most of the proposed ideas focus on the first approach, which is based on switching. Applications of the switched-beam antenna concept for MAC layer algorithms improvement are known from the literature [29]–[32], but apart from presenting limited insight into the physical layer, those approaches rely on simplified ideal antenna radiation patterns and do not consider realistic parameters, such as beamwidth, sidelobe level, backward radiation, or angular switching resolution. These aspects are critical for reliable assessment and appropriate design of both, the network topology and the future protocols. The other aspect that is broadly discussed in the literature is traffic optimization by proper network topology adaptation [21], [33]–[35]. This is mainly related to network slicing or clustering, where certain geographical rules are provided with respect to find the optimal packet routes that improve the overall network performance. Most of the mentioned research are focused on the concepts based on the IEEE 802.11 standard, where not all aspects related to dense WSNs operation, especially in harsh environments, are considered. An important aspect in industrial WSNs is the Quality of Service (QoS) of the routed links. The QoS aspect is imperative in providing a guaranteed end-to-end performance and it is especially demanded for real-time applications. While most of the routing algorithms focus on energy consumption and reliability, they ignore the real-time aspect [36] and assume that the traffic speed is sufficient to meet the required QoS. More detailed examination of modern heterogeneous WSNs based usually on the IEEE 802.15 standard that are used for IIoT solutions is required due to the limited hardware capabilities (simple low-cost end devices), much higher network density and demanding propagation environment. To address all the problems mentioned above, a novel approach that combines the concept of network layering presented in our work [37] and sensor nodes equipped with the electronically steerable parasitic array radiator (ESPAR) antenna [38]–[40] has been proposed in this article. In [37], a routing algorithm was presented that optimizes the energy consumption and minimizes the latency by searching an optimal routing scheme. In this work, we leave out the routing aspects and focus on finding an optimal layered network structure by introducing relay nodes equipped with ESPAR antennas and are capable to change the radiation pattern based on the network requirements [40]. Different from [37], we consider the link QoS to discover the network structure. By the boost of directional beams and the relaying, a stringent link QoS can be achieved. The discovered network structure can then be used in combination with various routing algorithms as the one in [37].

A. Contribution and Organization

Our contribution is summarized as in the following. First, we propose an algorithm that is capable to discover a hierarchical structure of the network sorted in layers of relays. This algorithm defines the relay nodes that comprise each layer and is centralized starting from the wireless network processor (WNP). Each layer of relay nodes is responsible to receive and forward the signal to the next layer. This approach creates room for further investigations into routing schemes, however such schemes are out of the scope of this work. Second, we propose a switched-beam ESPAR antenna that is capable to reconfigure the direction of radiation for directive beams or use the omnidirectional pattern. Key idea is to utilize both distance and spatial domains and reduce the number of layers or hops in the communication by still guaranteeing the link quality with a given threshold. For a relay node, it is possible to receive the signal while utilizing an omnidirectional radiation pattern and forward the signal with either a directional or omnidirectional pattern. We conducted measurements and incorporated the measured antenna radiation patterns for various configurations of ESPAR in our analysis. The main goal of this article is to analyze and evaluate the proposed hierarchical relay layering concept with the utilization of beam-switched antennas in scenarios relevant for WSN. For this, we consider a broad number of parameters, starting with various densities of the nodes, various propagation conditions, various requirements on the link quality, and various configurations of the ESPAR antenna, i.e., utilizing two, four, or more directional beams. We select two propagation models: 1) the free-space path loss (FSPL) model representing a best-case scenario in terms of propagation losses and 2) the two-slope path loss (TSPL) model representing a more realistic scenario blockages on the propagation paths. The two models serve as boundary between

TABLE I
MEASUREMENTS

n	V^n	φ^n_{max}
1	$V^1_{\max} = [111110000000]$	0°
2	$V^2_{\max} = [011111000000]$	30°
3	$V^3_{\max} = [001111100000]$	60°
4	$V^4_{\max} = [000111110000]$	90°
5	$V^5_{\max} = [000011111000]$	120°
6	$V^6_{\max} = [000001111100]$	150°
7	$V^7_{\max} = [000000111110]$	180°
8	$V^8_{\max} = [000000011111]$	210°
9	$V^9_{\max} = [100000001111]$	240°
10	$V^{10}_{\max} = [110000000111]$	270°
11	$V^{11}_{\max} = [111000000011]$	300°
12	$V^{12}_{\max} = [111100000001]$	330°
13	$V^{13}_{\text{omni}} = [000000000000]$	n/a

blockage-free and blockage-prone scenarios. Our analysis give simple rule of thumbs on the advantages and optimal configuration modes of the switched beam ESPAR antennas in industrial WSNs.

The remainder of this article is organized as follows: in Section II, the antenna concept and design is presented. In Section III, we provide the system model including the relay discovery algorithm as well as the model for link quality. Next, we analyze and discuss simulation results in Section IV, and at the end, in Section V, we discuss and draw our conclusions.

II. ANTENNA

A. Antenna Concept and Design

The antenna proposed for the experiment is an ESPAR antenna based on the design presented in [39]. It is a circular array, where a centrally located active monopole is surrounded by 12 passive elements mounted on a PCB with this metallic groundplane on the top layer. The passive elements are connected to the ground via digitally controlled integrated SPDT switches located at the bottom layer of the antenna. Depending on the switch state, each passive element can be short-circuited or open-circuited to the antenna groundplane and act as a reflector or a director, respectively, that stops or passes the electromagnetic wave. By proper combination of the switches states one can generate a directional radiation pattern that can be rotated by 0° to 360° with discreet step of 30°. A steering vector $V^n = [v_1, v_2, \ldots, v_{13}]$ has been introduced to describe the antenna radiation pattern configuration, where $v_1, v_2, \ldots, v_{13}$ are binary values representing the states of the passive elements of the array. A state of 1 indicates when the corresponding element is a director, whereas a state of 0 indicates a reflector. The antenna is able to operate in two radiation modes, with the mentioned directional beam $V_{\max}$ and the omnidirectional pattern V_{omni} that is obtained when all passive elements are directors, which, in total, gives $n = 13$ available radiation patterns (12 directional and 1 omnidirectional), as presented in Table I.

B. Realized Antenna

The fabricated antenna with dimensions is presented in Fig. 1. It has been realized on 1.55-mm thick FR4 substrate. The SMA connector has been used to feed the active monopole. The NJG1681MD7 FET SPDT switches have been used to realize the switching circuits (Fig. 1). They exhibit high isolation and low insertion loses and can be controlled with a typical microcontroller's or transceiver's GPIO with 2.5–5 V power supply. The switching circuits together with simple LED indicators have been located on the bottom layer of the fabricated PCB while the top layer forms the antenna ground. Antenna active and passive elements have been made of brass to keep the construction stable and less fragile and susceptible to mechanical damages.

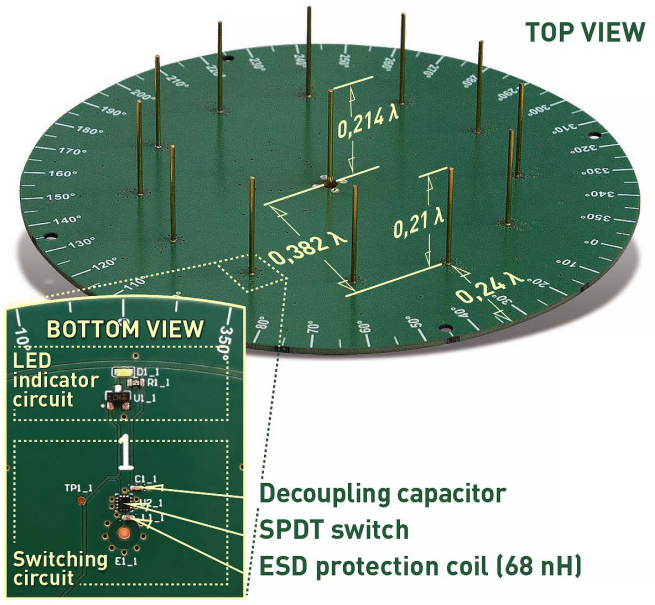

Fig. 1. Realized ESPAR antenna.

C. Measurements

The measured and simulated results are presented in Fig. 2. The measured half-power beamwidth (HPBW) of the directional configuration is equal to 75°, which is comparable with the simulated results. The main differences between simulation and measurement are for backward radiation and gain at $\theta = 90°$. Backward radiation level is 4-dB higher comparing to simulation while the measured gain is 1.7-dB lower than the simulated value. Similar discrepancies can be observed for the configuration with omnidirectional radiation pattern at some angles. The differences are caused mainly by the imperfect realization and nonideally mounted passive elements as well as the fact that only approximate value of the conductivity that was incorporated into the antenna model. These observations indicate the importance of realistic radiation patterns of the antenna to which one should resort in system simulation if more accurate results are expected.

III. SYSTEM MODEL

We consider a static WSN consisting of a single WNP denoted by N_0 and set of M sensor nodes $\{N_1, \ldots, N_M\}$ that

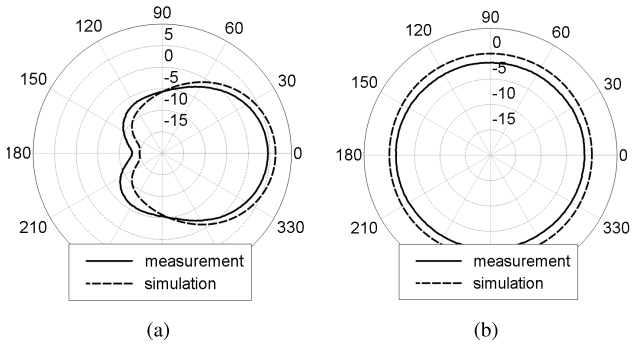

Fig. 2. Antenna radiation patterns for horizontal plane at $\theta = 90°$.

are synchronized and communicate using the time-division multiple access (TDMA)-based MAC protocol. All network elements are considered part of the set $\mathbf{S} = \{N_0, N_1, \ldots, N_M\}$. The sensor nodes are centrally managed by the WNP. We suppose that not all nodes can establish a direct communication link with the WNP, with a guaranteed QoS. This assumption is especially relevant for industrial communications, where the wireless channel experiences fading and link quality varies over time. Furthermore, the limitation in transmit power contributes in not having a stable direct communication between WNP and the nodes. In order to overcome such problems, we introduce a relaying concept based on a guaranteed QoS. In this way, a relay node is capable to receive the signal under a guaranteed QoS and forward it to the rest of the network. To determine whether a sensor node N_m is able to perform as a relay between WNP N_0 and other nodes in the network, the following condition is applied:

$$N_m = \begin{cases} \in \mathbf{R}, & \text{if } \zeta_{0m} \geq \mathrm{T} \\ \mathbf{S}\backslash\mathbf{R}, & \text{otherwise.} \end{cases} \tag{1}$$

The parameter ζ_{0m} denotes the link quality between nodes N_0 and N_m, and it can be any parameter that measures the link quality, such as the received signal strength indicator (RSSI), signal-to-noise ratio (SNR), received power, packet error rate, etc. A certain threshold indicated by T is considered in order to control the link quality and thus determine whether a node can act as a relay in the network. The subset $\mathbf{R}$ indicates relay nodes, whereas the nodes that can not meet the criteria to become a relay, are part of $\mathbf{S}\backslash\mathbf{R}$. We will refer to these nodes simply as *nonrelay nodes*.

The WNP and sensor nodes are equipped with an ESPAR antenna as introduced in Section II. We let the ESPAR antenna to have different configurations, an omnidirectional radiation pattern, or a directional radiation pattern that can be rotated between 0° and 360° with a step of 30°. In our system model we follow the assumption that after the nodes are synchronized, when in the listening mode, each sensor node utilizes the omnidirectional mode. When transmitting/forwarding, one can choose between omnidirectional and directional modes. One additional packet has to be sent each time there is a change in the configuration pattern. Figure 3 illustrates an example of a single WNP N_0 and three sensor nodes, where N_m is a relay node; whereas, N_p and N_q are nonrelays. The WNP transmits a signal utilizing a directional mode of antenna,

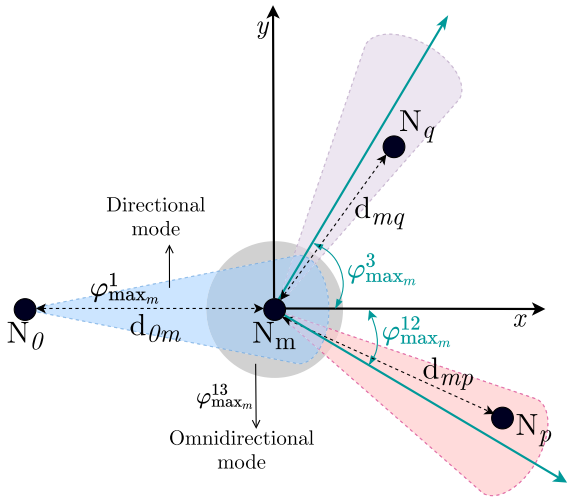

Fig. 3. Concept of relaying in a network with four nodes. Node N_0 is the WNP, node N_m is a relay, while N_p and N_q are nonrelay nodes.

while all other nodes that are in the listening mode employ an omnidirectional antenna pattern. The gray area denotes the omnidirectional mode applied when node N_m is in the listening mode and receives the signal from N_0. In the next step, node N_m acts as a relay and forwards the signal from N_0 to the rest of network nodes utilizing a directional mode of the ESPAR antenna. Two angular directions are depicted in the figure for illustration, $\varphi^3_{\max_m}$ and $\varphi^{12}_{\max_m}$. The light red area denotes the directional mode when node N_m is forwarding the signal received from N_0 to node N_p. Note that the directions of the ESPAR at node N_m are chosen for illustration purposes. In practice, node N_m would transmit in random directions depending on the configuration capabilities, i.e., switching between all 13 radiation pattern combinations, or switching between a few directions. In addition, we consider that node N_m is not aware of the location of other nodes in its surrounding. To determine which nodes are capable to act as relay, we introduce a recursive algorithm that classifies the network into layers or relaying.

A. Recursive Relay Discovery

In order to allow for a distributed network structure, based on the relaying concept from (1), we introduce a structured network connection concept that is organized in layers. The basic principle here is to apply a hierarchical algorithm that determines the sensor nodes that are capable to act as relays in the network. We refer to this as the *recursive relay discovery*. It starts from the central WNP, and in the first stage of the algorithm the WNP broadcasts a signal. Based on the link quality criteria from (1), the nodes from the set $\mathbf{S}_f = \mathbf{S}\backslash N_0$ that meet this criteria are marked as relay nodes and compose the first layer of relay nodes, denoted by the set $\mathbf{R}_1$. Algorithm 1 describes in more detail the first stage of the relay discovery performed at the WNP. When the algorithm starts, the parameter n denoting the actual layer is set to $n = 0$. For each discovered relay at this stage, the WNP is added in the list $\mathbf{B}$, denoting the list of all possible backward nodes for a discovered relay node. After the link quality criteria are applied

Algorithm 1 Network Discovery at WNP—Stage 1

$\mathbf{S} = \{N_0, N_1, \ldots N_M\}$
$\mathbf{S}_f = \mathbf{S} \backslash N_0$
$n = 0$
$\mathbf{R} = \emptyset$
$\mathbf{F} = \emptyset$
$\mathbf{B} = \emptyset$
for all $N_m \in \mathbf{S}_f$ **do**
  if N_m.relay $\leftarrow$ *true* **then**
    $\mathbf{R}_{n+1}$.append(N_m)
    $\mathbf{B}_{n+1}^{(N_m)} \leftarrow \mathbf{N}_0$
    $\mathbf{B}_{n+1}^{C}$.append($\mathbf{B}_{n+1}^{(N_m)}$)
    $\mathbf{S}_f \leftarrow \mathbf{S}_f \backslash \mathbf{R}_{n+1}$
$n \leftarrow 1$
return $n, \mathbf{R}_{n+1}, \mathbf{S}_f, \mathbf{B}_{n+1}^{C}$

Algorithm 2 Network Discovery at Node N—Stage 2

while $\mathbf{R}_n \neq \emptyset$ **do**
  for all $N_k \in \mathbf{R}_n$ **do**
    for all $N_f \in \mathbf{S}_f$ **do**
      if $\zeta_{kf} \geq \mathrm{T} \leftarrow$ *true* **then**
        $\mathbf{R}_{n+1}$.append(N_f)
        $\mathbf{B}_{n+1}^{(N_f)} \leftarrow \mathbf{N}_k$
        $\mathbf{F}_{n}^{(N_k)}$.append(N_f)
        $\mathbf{B}_{n+1}^{C}$.append($\mathbf{B}_{n+1}^{(N_f)}$)
        $\mathbf{F}_{n}^{C}$.append($\mathbf{F}_{n+1}^{(N_k)}$)
        $\mathbf{S}_f \leftarrow \mathbf{S}_f \backslash \mathbf{R}_{n+1}$
  $n \leftarrow n + 1$
return $n, \mathbf{R}_n, \mathbf{F}, \mathbf{B}, \mathbf{S}$

for each of the nodes in the set $\mathbf{S}_f$, the algorithm stops. In this step, the first layer of relays is known and parameter n is incremented to 1.

In the second stage, a recursive relay discovery starts, performed at the set of already discovered relays, i.e., $\mathbf{R}_1$-layer one. Algorithm 2 shows the procedure of selecting relays for each layer recursively. The algorithm starts with relay nodes discovered previously, and for each of these relay nodes $N_k \in \mathbf{R}_n$, the link quality between N_k and each of the free nodes from set $\mathbf{S}_f$ is compared with a given threshold T in order to determine the next layer relays. For each new listed relay node, the routing tables are updated denoting the possible backward nodes ($\mathbf{B}$), forward nodes ($\mathbf{F}$), new layer relays ($\mathbf{R}_{n+1}$), and the remaining set of free nodes ($\mathbf{S}_f$). After each iteration the index denoting the number of already discovered layers is incremented by one. The algorithm stops when the set of the possible discovered relay nodes in the new layer is empty $\mathbf{R}_n = \emptyset$. There are two possible cases, first that all free nodes from the set $\mathbf{S}_f$ meet the link quality threshold criteria and are listed as relays, and second, the free nodes form the set $\mathbf{S}_f$ do not meet the link quality criteria; therefore, they are marked as *nonrelay nodes*. This network structure is flexible to be applied in various routing algorithms, such as the one in [37]. It allows to optimize routes based on various criteria, such as energy efficiency, load balancing, delay, etc. In the reminder of this article, we only focus on determining the relay nodes based on the link quality and focus on the benefits of directional antennas for various network conditions.

B. Link Quality

By combining the path loss L(d), antenna gain $\mathrm{G}(\theta, \varphi)$, and transmit power P, a position-dependent large-scale fading can be obtained characterizing the propagation losses from a transmitter to a receiver location. We assume the noise power density σ_n^2 and consider unit transmit power P. The expression for the SNR for the link between nodes N_k and N_l can be written as

$$\zeta_{kl} = \frac{\mathrm{P}_k \mathrm{L}_{kl}(d) \mathrm{G}_k(\theta, \varphi)}{\sigma_n^2}. \quad (2)$$

To capture path loss L(d), we distinguish between two scenarios as follows.

1) *FSPL:* The ideal scenario with no obstructions in the propagation path between nodes, where the loss between two locations/radiators is the free space and for this, we consider the FSPL. The distance-dependent path loss is given by

$$\mathrm{L(d)}^{(\mathrm{FSPL})} = 21.98 + 20\log_{10}(\lambda) - 20\log_{10}(d) \quad (3)$$

where d denotes the distance between two locations and λ is the wavelength.

2) *TSPL:* A loss-prone scenario representing industrial environments with big obstruction surfaces. For this, we employ a TSPL that is derived based on measurements in manufacturing facilities. The model distinguishes between line-of-sight (LOS) and Non LOS (NLOS) propagation by changing the slope of the propagation loss at a certain breakpoint distance. In particular, we consider a path-loss model derived from measurements carried out at the National Institute of Standards and Technology (NIST) Central Utility Plant [41], which is an indoor industrial steam generation plant consisting of large machinery, such as boilers and multiple metallic surfaces and overhead pipes. Such a scenario is realistic to represent industrial factories with a lot of machinery. The distance-dependent path loss is given by

$$\mathrm{L(d)}^{(\mathrm{TSPL})} = \begin{cases} p_1 10\log_{10}\left(\frac{1}{d}\right) - q_1, & d \leq d_{\mathrm{BP}} \\ p_2 10\log_{10}\left(\frac{1}{d}\right) \\ \quad - (q_2 + d_{\mathrm{BP}}(p_2 - p_1)), & d > d_{\mathrm{BP}} \end{cases} \quad (4)$$

where d denotes the distance between two locations. Parameters p_1 and p_2 represent path-loss exponents and q_1 and q_2 indicate the path gain at a certain distance form the transmitter. The parameter d_{BP} denotes the breakpoint distance indicating the distance where the slope of the path loss changes.

For the antenna gain $\mathrm{G}_k(\theta, \varphi)$, we employ the measured radiation pattern of the ESPAR antenna described in Section II. We consider only the antenna radiation pattern in the azimuth domain, i.e., at constant $\theta = 90°$.

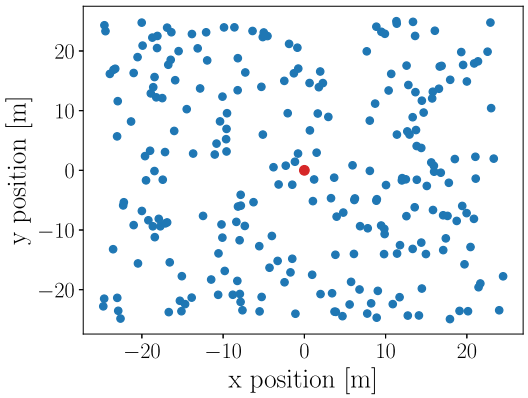

Fig. 4. Simulated scenario with a single WNP (in red) and sensor nodes (in blue) with density $\mu = 0.1$.

TABLE II
SIMULATION PARAMETERS [41, TABLE 4–2]

Parameter	Value
Frequency	2.245 GHz
ESPAR antenna	$\theta = 90°$, $\varphi \in [0°, 360°]$
Path loss exponent p_1	-1.1
Path loss exponent p_2	-2.6
Path gain q_1	-46
Path gain q_2	-30
Breakpoint distance d_{BP}	11

IV. PERFORMANCE INVESTIGATION

A. Simulation Setup

In this section, we evaluate the recursive relay discovery with the introduced setup in Section III and the measured antenna gain from Section II. We consider an area of 50 m×50 m, a single WNP located at the center of the area and a set of M sensor nodes uniformly distributed within this area. Figure 4 shows a simulated example of the network with 250 nodes. For the link quality modeling, we select the SNR as link quality measure and we follow the description in Section III-B. Since in our work, we consider a TDMA-based network with synchronized nodes, we assume an interference-free network. Another important aspect in the interference caused by the multipaths that arrive with a delay larger than the delay window corresponding to the length of a slot. According to [42], this interference is negligible and the SNR can be considered as an accurate approximation. Simulation parameters are given in Table II.

B. Analysis of Relay-Free Network

1) ESPAR Configuration Modes: In this part, we focus on the behavior of various ESPAR configurations before applying the network discovery algorithm. Fig. 5 illustrates the received power for a simulation area of 50 m×50 m and a single WNP located in the center. The WNP is equipped with an ESPAR antenna that can switch between five configurations: 1) omnidirectional; 2) two beams; 3) four beams; 4) six beams; and 5) 12 beams as indicated in Fig. 5. Similar configurations we use later to evaluate the network behavior of the relay discovery algorithm. For instance, in Fig. 5(c), the

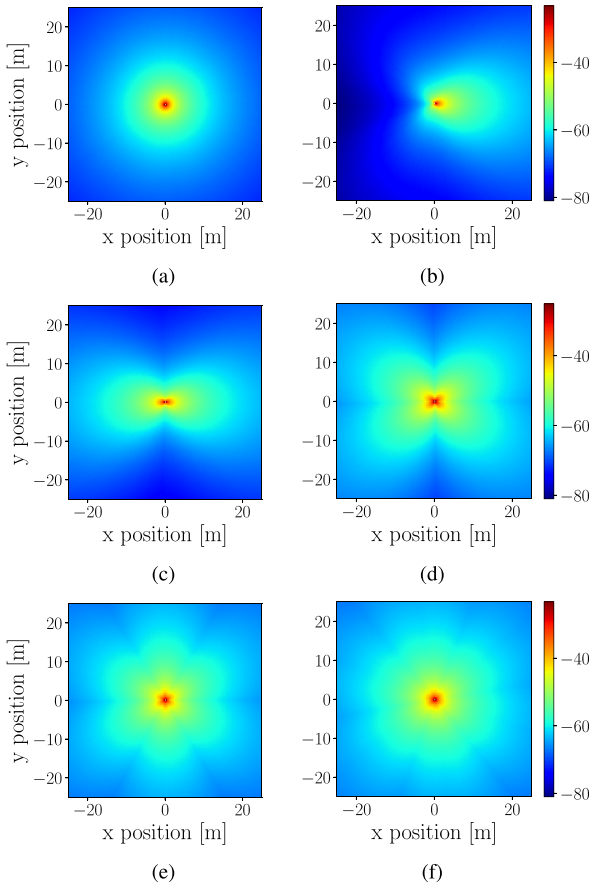

Fig. 5. Received power in dB for various ESPAR configurations $V^n_{\max}$ and $n \in \{1, 2, \ldots, 13\}$ as indicated in Table I. (a) Omnidirectional. (b) One beam. (c) Two beams. (d) Four beams. (e) Six beams. (f) 12 beams.

ESPAR antenna is set to have two reconfigurable radiation patterns pointing in different directions $V^{n_1}_{\max}$ and $V^{n_2}_{\max}$, e.g., $V^1_{\max}$ and $V^7_{\max}$. The beam direction is selected randomly such that $(n_1, n_2) \in \{1, 2, \ldots, 12\}$ and $n_1 \neq n_2$. The results indicate the changes in terms of the received power in different regions of the simulated area when switching from the omnidirectional mode to directional configurations. The use of directional beams in general improves the received power range when going from omnidirectional to directional mode. Furthermore, for a higher number of switching beams, the received power improves significantly not only for the locations close to the WNP but also at distant locations. For example, for six and 12 beams, the benefit of directional antenna gain results in reaching a value of around −60 dBm in terms of received power for a radial distance of 15 m from the central WNP, as compared to about 8 m achieved in the omnidirectional case for the same value of received power.

2) SNR Statistics: We consider the same simulation area as previously, a single WNP located in the center and $M = 1250$ sensor nodes that are uniformly distributed. All sensor nodes and the WNP utilize the omnidirectional mode of the ESPAR antenna. We perform simulations separately considering the two path-loss models, the FSPL, and the TSPL. For each of the two cases, we record the SNR of the broadcast links from WNP to each of the sensor nodes in the network. Figure 6

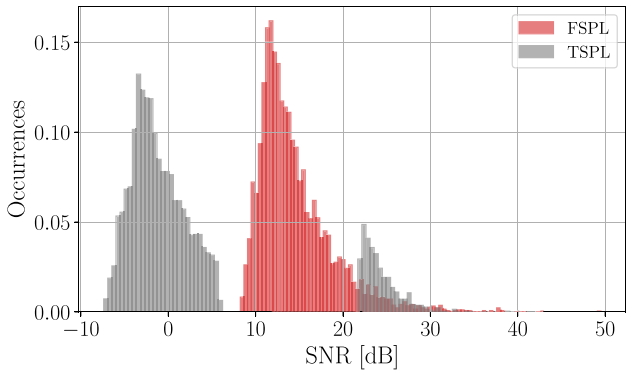

Fig. 6. SNR distribution for the two path-loss models and ESPAR omnidirectional mode.

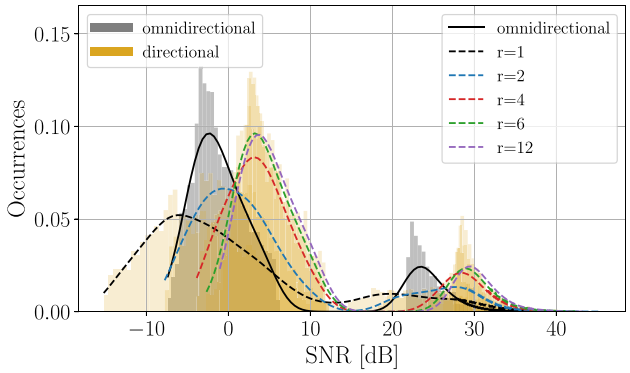

Fig. 7. SNR distribution for the TSPL and different ESPAR antenna settings, directional modes denoted by dashed lines for various r and omnidirectional denoted by solid line. Bars denote the actual occurrences, while lines denote the approximated distribution.

shows the distribution of the SNR for the two path-loss models. In the case of FSPL, the SNR statistics show that the samples are centered around 13 dB and follow a unimodal distribution. In contrary to the FSPL, we notice that for the NIST path-loss model the SNR follows a bimodal distribution, indicating two regions that are separated for about 15 dB: 1) the NLOS range (left) and 2) the LOS range (right). The gap between the two regions is caused by drop in received signal power at distances beyond the breakpoint distance, reflecting the blockages caused from the large metallic obstacles considered in this scenario. The given statistics are of importance to understand the impact of the SNR threshold on the routing discovery algorithm that we will discuss later on. Furthermore, Fig. 6 reflects the fact that we are considering two extreme cases of the propagation conditions: where with the FSPL, we target the best case scenarios, where there are no obstacles between sensor nodes, and the with the TSPL, we target the worst case scenarios, where there are a lot of big obstacles in the considered area. Any other scenario would stand in between the two cases we are considering.

Next, we switch the antenna at WNP to a directional mode and consider four configurations with the number of beams set to $r = \{2, 4, 6, 12\}$. Figure 7 shows the SNR distribution for the case of TSPL for various directional modes. The figure indicates how the SNR distribution changes when switching from omnidirectional to directional configuration. When switching from omnidirectional to directional mode considering one beam only, i.e., $r = 1$, we notice a deterioration in terms of SNR for the low SNR regime, and for the high SNR regime again we notice a shift toward lower values. This simply reflects the fact that a single directional antenna beam is not able to combat the omnidirectional case. When increasing the number of directional beams to $r = 2$, we start to notice an improvement compared to $r = 1$, but still only a slight improvement in terms of SNR is revealed for the low SNR as compared to the omnidirectional mode. Starting from $r = 4$, the SNR shifts to the right for both low and high SNR regimes and reaches a shift of around 8 dB for $r = \{6, 12\}$. Furthermore, the results reveal that $r = 6$ and $r = 12$ achieve almost the same behavior indicating that in a network without introducing a relay concept, the ESPAR antenna with directional mode already improves the SNR substantially, and that with a maximum of six redirectional beams.

C. Analysis of Relay-Aided Network

1) Number of Layers and Node Density: In this part, we put our focus on the relay discovery algorithm. We consider the same simulation area as before, a single WNP positioned at the center and vary the number of sensor nodes by considering three cases, $M = \{25, 250, 1250\}$. We represent the number of nodes M by the node density parameter, that for the simulation area of 50 m$\times$50 m, leads to $\mu = \{0.01, 0.1, 0.5\}$, respectively. The ESPAR antenna is set in the omnidirectional mode at both WNP and sensor nodes. We now apply the recursive relay discovery algorithm discussed in Section III-A and let the network discover its structure by defining layers of relay nodes. As a link quality measure and control parameter for the algorithm, we consider the SNR threshold T for each respective link. Obviously, the network structure will change depending on the value of T, therefore, we consider a broad range of thresholds $T = \{-10, -9, -8, \ldots, 43, 44\}$ dB and for each T value, we let the recursive discovery algorithm run and evaluate the maximum number of layers $n_{\max}$ that are reached. $n_{\max}$ directly impacts the multihop latency, therefore a lower $n_{\max}$ is desirable, whereas the threshold T determines the reliability of the network. The results in terms of $n_{\max}$ averaged over 500 simulation realizations are shown in Fig. 8 for the two path-loss models: 1) the FSPL in Fig. 8(a) and 2) TSPL in Fig. 8(b), respectively. The maximum number of layers (or hops) changes depending on the threshold T. In the case of the FSPL, the maximum number of hops for a node density $\mu = 0.01$ is achieved for $T = 19$ dB. When the threshold is very low, i.e., $T < 8$ dB, with the given network settings, all nodes can reach the threshold and, thus, become relays. These nodes are then assigned to layer 1. Therefore, the maximum number of layers reached for this SNR remains the same, $n_{\max} = 1$. When the threshold is in the range $8 \leq T \leq 19$ dB, the number of relay layers starts to increase. This indicates that in the first instance of the relay discovery algorithm, not all nodes in the network can reach threshold T, thus allowing more layers to be build. Next, for $19 < T < 24$ dB, the maximum number of layers starts to decrease. This stems from the

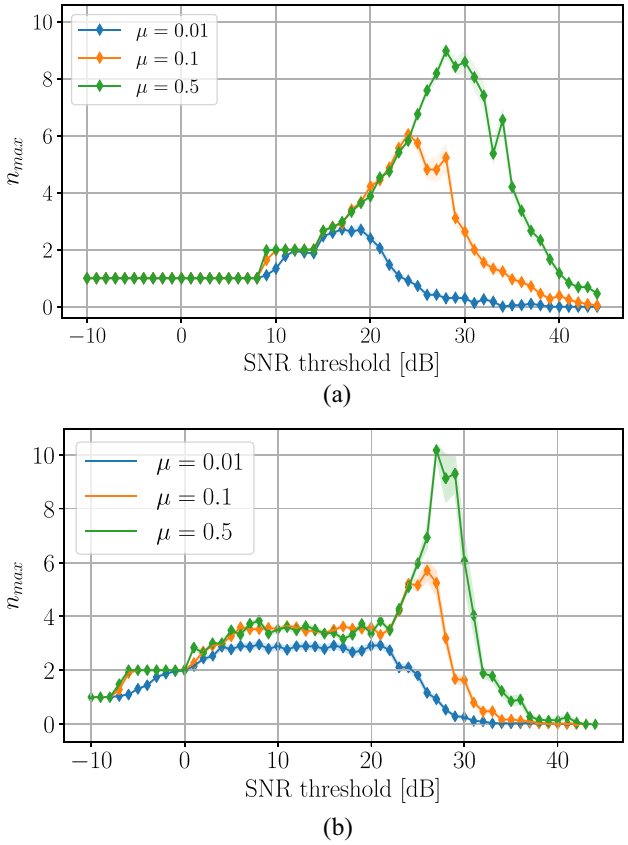

Fig. 8. Maximum number of layers for various user densities and an ESPAR omnidirectional setting. (a) FSPL. (b) NIST TSPL.

fact that the given threshold cannot be reached by some nodes in the network, in any instance (layer) of the discovery phase. In this case, there are always nodes in the network that are nonrelay per function. We will discuss the impact of various parameters on the number of nonrelay nodes later, in a separate section. In addition, when observing this behavior over node density, the results in Fig. 8(a) indicate that the maximum number of layers achieved is larger for higher node density. Furthermore, increasing the node density, the maximum for $n_{\max}$ occurs for higher threshold T, e.g., for $\mu = 0.1$, the $n_{\max}$ is reached for $T = 24$ dB, while for $\mu = 0.5$ for $T = 28$ dB. This comes due to the fact that with a higher node density, the distances between nodes get smaller; therefore, the SNR per link improves.

Similar behavior is achieved for the TSPL in Fig. 8(b). Contrary to the FSPL, there is a larger range of threshold T that provides more than a single layer of relays, i.e., $n_{\max} > 1$. This range is $-8 < T < 38$ dB, while for the FSPL it is $8 < T < 40$ dB. This behavior is due to the SNR distribution (see Fig. 6) that is affected by the two different path-loss models. It is important to note that in the case of TSPL, for node density $\mu = 0.1$ and $\mu = 0.5$, with the threshold values $T = 26$ dB and $T = 27$ dB, respectively, after the network discovery algorithm, each link in each layer is bounded to the high SNR regime, bringing the nodes to be in LOS. This is especially relevant for scenarios with a lot of obstructions, indicating that the introduced relaying concepts provides a guaranteed link quality even for scenarios with harsh propagation conditions, for a density of at least $\mu = 0.1$.

2) Number of Layers and Nonrelay Nodes for Various ESPAR Configurations: In this part, we focus on the impact of various configurations of the ESPAR antenna when incorporated to the relay discovery algorithm. In particular, we look at two parameters: 1) *the maximum number of layers* that can be obtained on average and 2) *the percentage of nonrelay nodes* in the network subject to threshold T, environment type described by the two path-loss models and ESPAR antenna type. We consider the simulation setup from Section IV-A with three node densities $\mu = \{0.01, 0.1, 0.5\}$ and ESPAR antenna that uses omnidirectional mode and directional mode with number of beams $r = \{2, 4, 6, 12\}$. We perform the analysis separately for FSPL and TSPL path-loss models. The results for the case of FSPL are shown in Fig. 9. In the following, we outline the most important findings.

1) For low node density of $\mu = 0.01$ shown in Fig. 9(a), switching from omnidirectional to directional mode decreases the number of relay layers for about one layer less, depending on the number of beams r. It can be noted that for $r > 4$, the differences in terms of $n_{\max}$ are not that significant anymore. This reveals that by increasing the number of beams r, under the same threshold T and a guaranteed link quality, less hops/layers of relaying are sufficient to keep the network link quality T. A lower number of layers contributes to smaller delays in forwarding the packets, therefore is desirable in WSNs. On the other side, when observing the percentage of nodes in the network that result to be nonrelays, because of not being able to meet the link quality threshold criteria, this percentage increases over the applied threshold T when switching from omnidirectional to directional mode. Furthermore, increasing the number of directional beams r results into a lower number of nonrelay nodes for respective threshold T. This indicates that there is a tradeoff between number of layers and nonrelay nodes for a given range of threshold T.
2) For node density $\mu = 0.1$ given in Fig. 9(c), the difference between omnidirectional and directional mode significantly increases. Switching from omnidirectional to $r = 2$ already decreases the maximum number of layers by 50%. As for the number of directional beams, one can notice that for $r > 4$, there is no significant change anymore. When observing the percentage of nonrelay nodes shown in Fig. 9(d), we notice less differences between omnidirectional and directional mode with various r. Only for $T > 25$ dB, the directional mode is more favorable. Otherwise, which mode to select depends on whether a higher number of hops in the network is desirable or not.
3) For highly dense networks with $\mu = 0.5$, switching from omnidirectional to a directional mode decreases the number of layers by 65%. The results indicate that in terms of number of layers, the benefit of directional ESPAR antenna is most significant in the networks with high density of the nodes. This reflects the benefit of ESPAR antenna gain, particularly in the scenarios, where

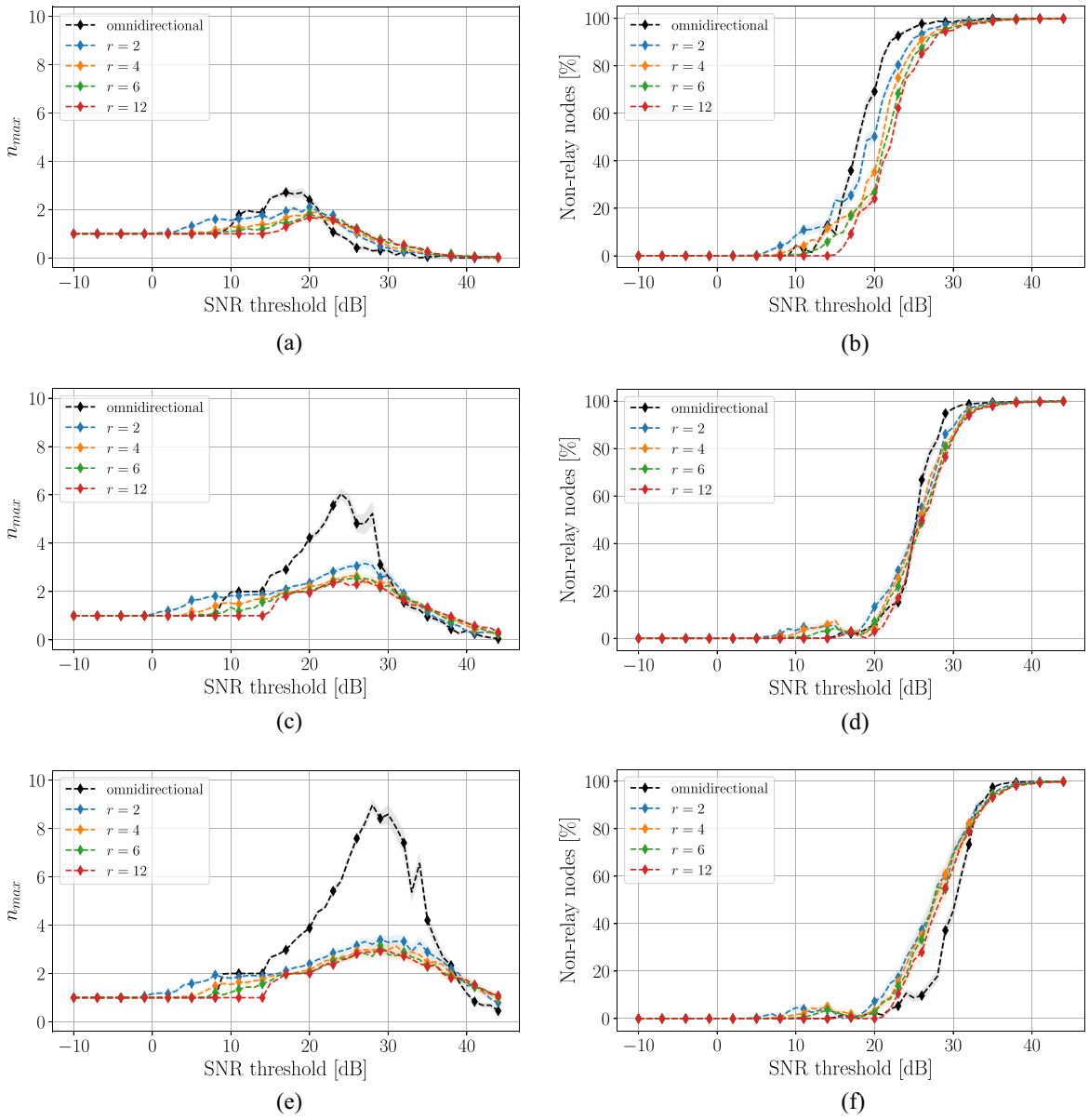

Fig. 9. Maximum number of layers and percentage of nonrelay nodes for different node densities and ESPAR configurations considering the FSPL path-loss model. The light shaded area denotes the 95% confidence interval. (a) Density $\mu = 0.01$. (b) Density $\mu = 0.01$. (c) Density $\mu = 0.1$. (d) Density $\mu = 0.1$. (e) Density $\mu = 0.5$. (f) Density $\mu = 0.5$.

sensor nodes are closely located. However, the results in terms on nonrelay nodes given in Fig. 9(f) indicate that for threshold values $T < 20$ dB, both omnidirectional and directional modes are optimal, while for $T > 20$ dB, the omnidirectional mode provides up to 20% less nonrelay nodes.

Next, we carry out similar analysis for the case of TSPL. The results are summarized in Fig. 10. In the following, we outline the most important findings.

1) For low node density $\mu = 0.01$ shown in Fig. 10(a), switching from omnidirectional to directional mode does not significantly impact the maximum number of relay layers. One can notice a slight decrease on $n_{\max}$ when going from omnidirectional to directional mode with various number of beams r. Another difference is the range of threshold T for which at least a single layer of relays exist. This is especially noticed on the high SNR range $25 < T < 35$ dB, indicating that the directional beams boost the link quality and therefore enable to reach at least one layer of relays, while for the same range with omnidirectional antenna, no relay layer is obtained. This means that with an omnidirectional antenna, it is not possible to keep a very good link quality ($T > 25$ dB). On the other side, when looking at the percentage of nonrelay nodes shown in Fig. 10(b), two things can be noticed. First, the omnidirectional mode outperforms the directional one for threshold values in the high SNR regime, making it favorable for $10 < T < 25$ dB. Second, considering the high SNR regime for threshold T, this comes in the expense of

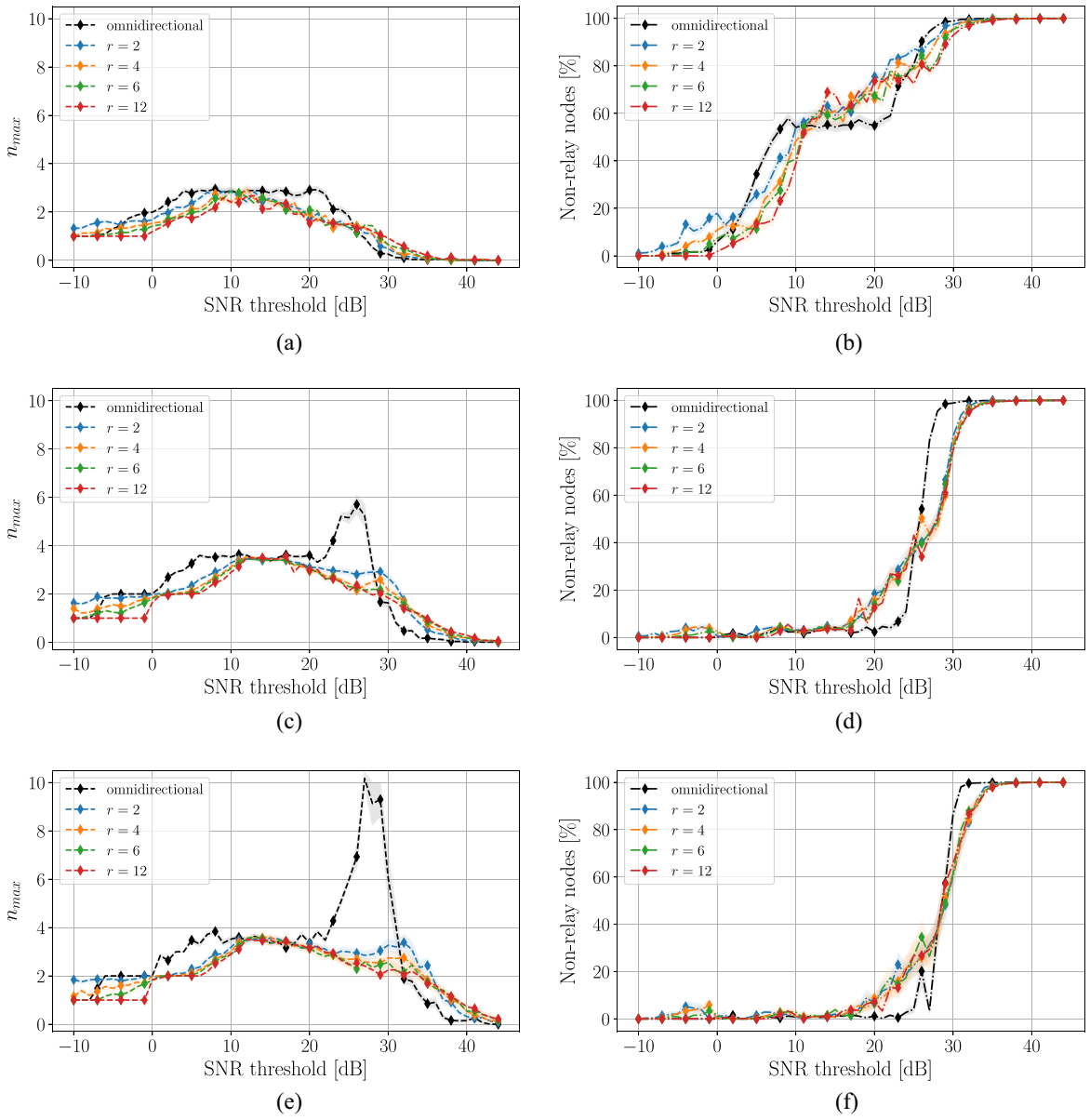

Fig. 10. Maximum number of layers and percentage of nonrelay nodes for different node densities and ESPAR configurations considering the TSPL path-loss model. The light shaded area denotes the 95% confidence interval. (a) Density $\mu = 0.01$. (b) Density $\mu = 0.01$. (c) Density $\mu = 0.1$. (d) Density $\mu = 0.1$. (e) Density $\mu = 0.5$. (f) Density $\mu = 0.5$.

more than 50% on nodes not being able to fulfill the link quality condition to become relay. Therefore, for a routing scheme, where it is important to have more possible routes rather than a higher link quality, this is only possible for $T < 5$ dB, assuring that at least 80% of the nodes are able to act a relay. This reveals that in a scenario prone to lots of blockages and with large distances between the nodes, there is no benefit in utilizing the directional mode.

2) For the node density $\mu = 0.1$ given in Fig. 10(c), the difference between omnidirectional and directional modes is more obvious. At a certain range of threshold T, the maximum number of layers for omnidirectional mode reaches up to six layers, while for directional mode, $n_{\max}$ is at least two times lower. This reveals that in terms of the number of layers, a reduction of 50% can be achieved by switching from omnidirectional to directional mode with only two beams ($r = 2$). By increasing the number of beams $r > 2$, this reduction increases even further. However, it is important to note that utilizing an ESPAR antenna with more than four beams does not lead to further significant improvements. When looking at the percentage of nonrelay nodes given in Fig. 10(d), the omnidirectional mode provides better results in terms of a lower number of nonrelay nodes for $T < 25$ dB. Therefore, for such a network setting, an omnidirectional mode is advisable. If a higher link quality is the goal, then directional modes becomes more suitable, however in the expense of less relay nodes available.

3) For highly dense networks with $\mu = 0.5$, the difference between omnidirectional and directional modes significantly increases. A switching from omnidirectional to directional mode results in up to 70% reduction in the maximum number of layers. This comes from the fact that, in highly dense networks, the distances between nodes are smaller and, in consequence, the impact of directional beams in the achieved SNR becomes more significant. Furthermore, for such dense networks, the benefit of ESPAR antenna with directional beams is in significantly reducing the number of hops, which in such dense networks becomes a crucial parameter. On the other hand, the percentage of nonrelay nodes shown in Fig. 10(f) indicates that for $T < 18$ dB, both antenna modes provide the same performance, while for $18 < T < 28$ dB, the directional mode causes up to 20% nonrelay nodes; therefore, omnidirectional mode becomes more favorable in terms of having more relay nodes. For $T > 28$ dB, the directional mode is always favorable.

V. Discussion and Concluding Remarks

The IIoT domain, where machinery is equipped with a number of connected sensors, efficient operation and at the same time safe requires reliable secure and dependable wireless communication. Since most of the industrial sites in IIoT are deployed indoors surrounded by many metallic components, the wireless communication becomes challenging due to harsh propagation conditions. Providing stable communication parameters in such an environment has been already broadly addressed in the literature by proposing proper protocols and using different routing algorithms. However, some limitations are not possible to mitigate only with the improvements on higher protocol layers and have to consider improvements on the physical layer as well. In this article, we examined the problem of link quality impairment on typical industrial sites due to harsh propagation conditions and assess link quality improvements with switched-beam ESPAR antennas and a layered structure of the network introducing relaying nodes.

In our TDMA network comprised of sensor nodes and one WNP, we introduce a switched beam ESPAR antenna, which is a circular array, and by proper combination of the switches state can generate a directional radiation pattern that can be rotated from 0° to 360°. The same antenna is also capable to operate in an omnidirectional mode. With the relay discovery algorithm presented in this article, we show how the network can benefit most by introducing sensor nodes that act as relay and utilize directional or omnidirectional radiation patterns. For a node to be a relay, it has to fulfill certain criteria such as having a defined link quality. Overall, the improvements in reducing the number of layers or hops are significant for all directional ESPAR configuration in free space as well as blockage-prone propagation conditions. On the one hand, utilizing the directional mode with just as low as two switching beams, can reduce the number of layers up to 65% in the case of FSPL and about 70% for the TSPL. The lower the node density, implying a larger separation in the location of the nodes, this reduction in terms of layers decreases. On the other hand, aiming for a better link quality set as controlling parameter for the relay discovery algorithm, there is clearly a tradeoff between having a high SNR per link and the percentage of nodes that can serve as relays. Our results reveal that if a lower number of layers is desirable for a network design, then in order to achieve a higher QoS (< 15 dB), directional beams are favorable. A lower number of layers is favorable in terms of minimizing the latency in a multihop communication. In addition, our results show that for certain scenarios going with a high QoS (> 30 dB), less relay nodes are available in the network. This range when about 50% of the nodes or more are not relaying the traffic might be a drawback for networks that aim to have an energy balance between nodes such that the load distribution does not vary a lot. Therefore, which QoS range to select will depend on the tradeoff between latency, energy consumption, and reliability in a network. Furthermore, our findings reveal that using a switched beam ESPAR antenna with a maximum of four beams is sufficient to achieve a high SNR and largely reduce the number of hops in wireless communication among WSN nodes.

Acknowledgment

The document reflects only the author's view and the Commission is not responsible for any use that may be made of the information it contains.

References

[1] S. Vitturi, C. Zunino, and T. Sauter, "Industrial communication systems and their future challenges: Next-generation Ethernet, IIoT, and 5G," *Proc. IEEE*, vol. 107, no. 6, pp. 944–961, Jun. 2019.

[2] M. Wollschlaeger, T. Sauter, and J. Jasperneite, "The future of industrial communication: Automation networks in the era of the Internet of Things and industry 4.0," *IEEE Ind. Electron. Mag.*, vol. 11, no. 1, pp. 17–27, Mar. 2017.

[3] A. Willig, K. Matheus, and A. Wolisz, "Wireless technology in industrial networks," *Proc. IEEE*, vol. 93, no. 6, pp. 1130–1151, Jun. 2005.

[4] J. R. Moyne and D. M. Tilbury, "The emergence of industrial control networks for manufacturing control, diagnostics, and safety data," *Proc. IEEE*, vol. 95, no. 1, pp. 29–47, Jan. 2007.

[5] M. Luvisotto, Z. Pang, and D. Dzung, "High-performance wireless networks for industrial control applications: New targets and feasibility," *Proc. IEEE*, vol. 107, no. 6, pp. 1074–1093, Jun. 2019.

[6] E. Sisinni, A. Saifullah, S. Han, U. Jennehag, and M. Gidlund, "Industrial Internet of Things: Challenges, opportunities, and directions," *IEEE Trans. Ind. Informat.*, vol. 14, no. 11, pp. 4724–4734, Nov. 2018.

[7] V. C. Gungor and G. P. Hancke, "Industrial wireless sensor networks: Challenges, design principles, and technical approaches," *IEEE Trans. Ind. Electron.*, vol. 56, no. 10, pp. 4258–4265, Oct. 2009.

[8] T. P. Raptis, A. Passarella, and M. Conti, "A survey on industrial Internet with ISA100 wireless," *IEEE Access*, vol. 8, pp. 157177–157196, 2020.

[9] V. Ç. Güngör and G. P. Hancke, *Industrial Wireless Sensor Networks: Applications, Protocols, and Standards*. Boca Raton, FL, USA: CRC Press, 2013.

[10] Q. Wang and J. Jiang, "Comparative examination on architecture and protocol of industrial wireless sensor network standards," *IEEE Commun. Surveys Tuts.*, vol. 18, no. 3, pp. 2197–2219, 3rd Quart., 2016.

[11] S. Li, S. Zhao, X. Wang, K. Zhang, and L. Li, "Adaptive and secure load-balancing routing protocol for service-oriented wireless sensor networks," *IEEE Syst. J.*, vol. 8, no. 3, pp. 858–867, Sep. 2014.

[12] F. Ferrari, M. Zimmerling, L. Thiele, and O. Saukh, "Efficient network flooding and time synchronization with glossy," in *Proc. 10th ACM/IEEE Int. Conf. Inf. Process. Sens. Netw.*, Chicago, IL, USA, 2011, pp. 73–84.

[13] A. A. Kumar S., K. Ovsthus, and L. M. Kristensen, "An industrial perspective on wireless sensor networks—A survey of requirements, protocols, and challenges," *IEEE Commun. Surveys Tuts.*, vol. 16, no. 3, pp. 1391–1412, 3rd Quart., 2014.

[14] M. Nobre, I. Silva, and L. A. Guedes, "Routing and scheduling algorithms for WirelessHARTNetworks: A survey, (Basel, Switzerland)" *Sensors*, vol. 15, no. 5, pp. 9703–9740, 2015.

[15] D. V. Queiroz, M. S. Alencar, R. D. Gomes, I. E. Fonseca, and C. Benavente-Peces, "Survey and systematic mapping of industrial wireless sensor networks," *J. Netw. Comput. Appl.*, vol. 97, pp. 96–125, Nov. 2017. [Online]. Available: http://www.sciencedirect.com/science/article/pii/S1084804517302771

[16] S. Shakkottai, T. S. Rappaport, and P. C. Karlsson, "Cross-layer design for wireless networks," *IEEE Commun. Mag.*, vol. 41, no. 10, pp. 74–80, Oct. 2003.

[17] U. C. Kozat, I. Koutsopoulos, and L. Tassiulas, "A framework for cross-layer design of energy-efficient communication with QoS provisioning in multi-hop wireless networks," in *Proc. IEEE INFOCOM*, vol. 2. Hong Kong, 2004, pp. 1446–1456.

[18] E. D. Skiani, S. A. Mitilineos, and S. C. A. Thomopoulos, "A study of the performance of wireless sensor networks operating with smart antennas," *IEEE Antennas Propag. Mag.*, vol. 54, no. 3, pp. 50–67, Jun. 2012.

[19] T. G. Shivapanchakshari and H. S. Aravinda, "Review of research techniques to improve system performance of smart antenna," *Open J. Antennas Propag.*, vol. 5, no. 2, p. 83, 2017.

[20] S. Ciccia, G. Giordanengo, and G. Vecchi, "Energy efficiency in IoT networks: Integration of reconfigurable antennas in ultra low-power radio platforms based on system-on-chip," *IEEE Internet Things J.*, vol. 6, no. 4, pp. 6800–6810, Aug. 2019.

[21] Y.-C. Chen and C.-Y. Wen, "Distributed clustering with directional antennas for wireless sensor networks," *IEEE Sensors J.*, vol. 13, no. 6, pp. 2166–2180, Jun. 2013.

[22] J. Zhang, S.-J. Liu, P.-W. Tsai, F.-M. Zou, and X.-R. Ji, "Directional virtual backbone based data aggregation scheme for wireless visual sensor networks," *PLoS ONE*, vol. 13, no. 5, pp. 1–27, May 2018. [Online]. Available: https://doi.org/10.1371/journal.pone.0196705

[23] Y.-C. Chen, P.-L. Chung, and C.-Y. Wen, "On autonomous clustering in wireless sensor networks with directional antennas," in *Proc. 4th Int. Conf. Sens. Technol. Appl.*, Venice, Italy, 2010, pp. 531–538.

[24] E. Felemban *et al.*, "SAMAC: A cross-layer communication protocol for sensor networks with sectored antennas," *IEEE Trans. Mobile Comput.*, vol. 9, no. 8, pp. 1072–1088, Aug. 2010.

[25] O. Bazan and M. Jaseemuddin, "A survey on MAC protocols for wireless adhoc networks with beamforming antennas," *IEEE Commun. Surveys Tuts.*, vol. 14, no. 2, pp. 216–239, 2nd Quart., 2012.

[26] H.-N. Dai, K.-W. Ng, M. Li, and M.-Y. Wu, "An overview of using directional antennas in wireless networks," *Int. J. Commun. Syst.*, vol. 26, no. 4, pp. 413–448, 2013. [Online]. Available: https://onlinelibrary.wiley.com/doi/abs/10.1002/dac.1348

[27] G. Giorgetti, A. Cidronali, S. K. S. Gupta, and G. Manes, "Exploiting low-cost directional antennas in 2.4 GHz IEEE 802.15.4 wireless sensor networks," in *Proc. Eur. Conf. Wireless Technol.*, Munich, Germany, 2007, pp. 217–220.

[28] G. Giorgetti, A. Cidronali, S. K. S. Gupta, and G. Manes, "Exploiting low-cost directional antennas in 2.4 GHz IEEE 802.15.4 wireless sensor networks," in *Proc. Eur. Conf. Wireless Technol.*, 2007, pp. 217–220, doi: 10.1109/ECWT.2007.4403985.

[29] T. Korakis, G. Jakllari, and L. Tassiulas, "A MAC protocol for full exploitation of directional antennas in ad-hoc wireless networks," in *Proc. 4th ACM Int. Symp. Mobile Ad Hoc Netw. Comput.*, 2003, pp. 98–107. [Online]. Available: https://doi.org/10.1145/778415.778428

[30] Z. Zhang, "DTRA: Directional transmission and reception algorithms in WLANS with directional antennas for QoS support," *IEEE Netw.*, vol. 19, no. 3, pp. 27–32, May/Jun. 2005.

[31] M. Takata, M. Bandai, and T. Watanabe, "A receiver-initiated directional MAC protocol for handling deafness in ad hoc networks," in *Proc. IEEE Int. Conf. Commun.*, vol. 9. Istanbul, Turkey, 2006, pp. 4089–4095.

[32] Y. Li and A. Safwat, "On wireless ad hoc networks with directional antennas: Efficient collision and deafness avoidance mechanisms," *EURASIP J. Wireless Commun. Netw.*, vol. 2008, Jun. 2008, Art. no. 867465. [Online]. Available: https://doi.org/10.1155/2008/867465

[33] I. Yoon, D. K. Noh, and H. Shin, "Multi-layer topology control for long-term wireless sensor networks," *EURASIP J. Wireless Commun. Netw.*, vol. 2012, no. 1, p. 164, 2012. [Online]. Available: https://doi.org/10.1186/1687-1499-2012-164

[34] D. T. C. Wong, Q. Chen, and F. Chin, "Directional medium access control (MAC) protocols in wireless ad hoc and sensor networks: A survey," *J. Sens. Actuat. Netw.*, vol. 4, no. 2, pp. 67–153, 2015.

[35] W. Zhang, X. Wei, G. Han, and X. Tan, "An energy-efficient ring cross-layer optimization algorithm for wireless sensor networks," *IEEE Access*, vol. 6, pp. 16588–16598, 2018.

[36] K. R. Venugopal, T. S. Prakash, and M. Kumaraswamy, in *QoS Routing Algorithms for Wireless Sensor Networks*, 1st ed. Singapore: Springer, 2020, doi: 10.1007/978-981-15-2720-3.

[37] H. Bernhard, A. Springer, P. Priller, and L. B. Hörmann, "Energy balanced routing for latency minimized wireless sensor networks," in *Proc. 14th IEEE Int. Workshop Factory Commun. Syst. (WFCS)*, Imperia, Italy, Jun. 2018, pp. 1–9.

[38] H. Kawakami and T. Ohira, "Electrically steerable passive array radiator (ESPAR) antennas," *IEEE Antennas Propag. Mag.*, vol. 47, no. 2, pp. 43–50, Apr. 2005.

[39] L. Kulas, "RSS-based DoA estimation using ESPAR antennas and interpolated radiation patterns," *IEEE Antennas Wireless Propag. Lett.*, vol. 17, pp. 25–28, 2018.

[40] M. Groth, M. Rzymowski, K. Nyka, and L. Kulas, "ESPAR antenna-based WSN node with DoA estimation capability," *IEEE Access*, vol. 8, pp. 91435–91447, 2020.

[41] "NIST channel sounder overview and channel measurements in manufacturing facilities," Nat. Inst. Stand. Technol., Gaithersburg, MD, USA, Rep. 1979, 2017.

[42] X. Jiang, Z. Pang, M. Luvisotto, R. Candell, D. Dzung, and C. Fischione, "Delay optimization for industrial wireless control systems based on channel characterization," *IEEE Trans. Ind. Informat.*, vol. 16, no. 9, pp. 5855–5865, Sep. 2020.

Fjolla Ademaj (Member, IEEE) received the M.Sc. degree (Hons.) in electrical engineering from the Faculty of Electrical and Computer Engineering, University of Prishtina, Pristina, Kosovo, in 2014, and the Dr.Techn. degree (Ph.D. equivalent) (Hons.) in telecommunications engineering from Technische Universitaet (TU) Wien, Vienna, Austria, in 2019.

From 2014 to 2019, she was a Project Assistant with the Institute of Telecommunications, TU Wien, where she co-developed the Vienna LTE-A and 5G system level simulators. From 2019, she is with Silicon Austria LABs GmbH, Graz, Austria, research center working as a Postdoctoral Researcher. Her research interests include wireless communications, system level modeling and simulations, channel modeling, and signal processing.

Mateusz Rzymowski (Member, IEEE) received the M.Sc. degree in microwave engineering from Gdansk University of Technology (GUT), Gdansk, Poland, in 2010.

He is currently a Researcher with the Department of Microwave and Antenna Engineering, GUT, organizing and conducting research for EU companies within EU-funded Research and Development projects. His main interests include reconfigurable antennas, millimeter wave antenna design, and security mechanisms that can be implemented in physical layer of wireless systems.

Hans-Peter Bernhard (Senior Member, IEEE) received the master's degree in electrical engineering and the Ph.D. degree in technical sciences from Technische Universitaet (TU) Wien, Vienna, Austria, in 1991 and 1997, respectively.

He is an Assistant Professor with TU Wien until 1998 and joined the Johannes Kepler University (JKU), Linz, Austria, as a Lecturer in 1999. In 2014, he started as a Senior Scientist with JKU and the Silicon Austria Labs, Linz, in 2018 as a Principal Scientist and the Head of Research Unit Wireless Communications. He has been a Visiting Researcher with the Prague Academy of Sciences, Prague, Czechia, and the University of Cambridge, Cambridge, U.K. His research interests include the design and analysis of time sensitive communication systems with a focus to resilient solutions.

Dr. Bernhard has given several invited talks on various aspects of wireless factory communication and is active in organizing IEEE and ACM conferences and workshops in various chair roles. He is a member of IES, TC-FA, and TC-II.

Krzysztof Nyka (Senior Member, IEEE) received the M.Sc. and Ph.D. degrees (Hons.) from Gdansk University of Technology, Gdansk, Poland, in 1984 and 2002, respectively.

He is currently an Associate Professor with the Department of Microwave and Antenna Engineering, Gdansk University of Technology. He has been very actively cooperating with industry partners within many national and EU projects. His research interests include computational electrodynamics, especially the application of model order reduction in finite-element method for efficient CAD tools, and microwave and millimeter wave circuits, and reconfigurable antennas for secure wireless applications.

Lukasz Kulas (Senior Member, IEEE) received the M.Sc. and Ph.D. degrees (Hons.) in microwave engineering from Gdansk University of Technology (GUT), Gdansk, Poland, in 2001 and 2007, respectively.

He currently holds an Associate Professor with the Department of Microwave and Antenna Engineering, GUT. He actively cooperates with EU industry within a numerous Research and Development projects. His main interests are reconfigurable antennas, direction-of-arrival algorithms, wireless embedded devices, and Internet-of-Things solutions that can be applied in practical industrial applications.